Available online at www.sciencedirect.com
ScienceDirect
Journal of the Mechanics and Physics of Solids
54 (2006) 2436–2452

JOURNAL OF THE MECHANICS AND PHYSICS OF SOLIDS

www.elsevier.com/locate/jmps

A cohesive law for carbon nanotube/polymer interfaces based on the van der Waals force

L.Y. Jiang[a], Y. Huang[a,*], H. Jiang[b], G. Ravichandran[c], H. Gao[d], K.C. Hwang[e], B. Liu[e]

[a]*Department of Mechanical and Industrial Engineering, University of Illinois, Urbana, IL 61801, USA*
[b]*Department of Mechanical and Aerospace Engineering, Arizona State University, Tempe, AZ, 85287, USA*
[c]*Graduate Aeronautical Lab, California Institute of Technology, Pasadena, CA 91125, USA*
[d]*Division of Engineering, Brown University, Providence, RI 02912, USA*
[e]*Department of Engineering Mechanics, Tsinghua University, Beijing 100084, PR China*

Received 17 February 2006; received in revised form 28 April 2006; accepted 29 April 2006

Abstract

We have established the cohesive law for interfaces between a carbon nanotube (CNT) and polymer that are not well bonded and are characterized by the van der Waals force. The tensile cohesive strength and cohesive energy are given in terms of the area density of carbon nanotube and volume density of polymer, as well as the parameters in the van der Waals force. For a CNT in an infinite polymer, the shear cohesive stress vanishes, and the tensile cohesive stress depends only on the opening displacement. For a CNT in a finite polymer matrix, the tensile cohesive stress remains the same, but the shear cohesive stress depends on both opening and sliding displacements, i.e., the tension/shear coupling. The simple, analytical expressions of the cohesive law are useful to study the interaction between CNT and polymer, such as in CNT-reinforced composites. The effect of polymer surface roughness on the cohesive law is also studied.

Keywords: Carbon nanotube composites; Cohesive law; Carbon nanotube/polymer interface; van der Waals force

*Corresponding author.
E-mail address: huang9@uiuc.edu (Y. Huang).

0022-5096/$ - see front matter © 2006 Elsevier Ltd. All rights reserved.
doi:10.1016/j.jmps.2006.04.009

1. Introduction

Carbon nanotubes (CNT) display superior mechanical properties, and have been used as reinforcements in polymer matrix composites (e.g., Thostenson et al., 2001, 2005; Maruyama and Alam, 2002; Deepak et al., 2003; Breuer and Sundararaj, 2004; Harris, 2004). Carbon nanotubes usually do not bond well to polymers (Schadler et al., 1998; Ajayan et al., 2000; Lau and Shi, 2002) such that their interaction is the van der Waals force (Liao and Li, 2001; Frankland et al., 2002; Li and Chou, 2003; Wong et al., 2003; Gou et al., 2004), which is much weaker than covalent bonds. This leads to sliding of CNT in polymer matrix when subjected to loading.

Continuum models have been developed for CNT-reinforced polymer matrix composites (e.g., Odegard et al., 2002, 2003; Liu and Chen, 2003; Li and Chou, 2003; Thostenson and Chou, 2003; Shi et al., 2004). As compared to atomistic simulations such as molecular dynamics, continuum models are not constrained on the length and time scales, and are suitable for the study of nanocomposites. However, modeling of CNT/polymer interfaces has always been a challenge because it is difficult to account for the van der Waals force in continuum models.

Cohesive zone models have been widely used in the continuum study of interface debonding and sliding in composites (e.g., Needleman, 1987; Camacho and Ortiz, 1996; Geubelle and Baylor, 1998). A cohesive zone model assumes a relation between the normal (and shear) traction(s) and the opening (and sliding) displacement(s). When implemented in the finite element method, the cohesive zone model is capable of simulating interface debonding and sliding (e.g., Huang and Gao, 2001; Zhang et al., 2002; Kubair et al., 2002, 2003; Samudrala et al., 2002, 2003; Thiagarajan et al., 2004a, b; Tan et al., 2005a, b, 2006). The existing cohesive models are all phenomenological because it is difficult to measure directly the cohesive laws for interfaces. There are some recent experimental studies of microscale cohesive laws (e.g., Li et al., 1987; Guo et al., 1999; Mohammed and Liechti, 2000; Bazant, 2002; Elices et al., 2002; Hong and Kim, 2003; Tan et al., 2005b), but none on nanoscale cohesive laws such as the CNT/polymer interfaces.

The purpose of this paper is to establish a cohesive law for CNT/polymer interfaces directly from the van der Waals force. It focuses on the van der Waals force, and does not consider the possible chemical bonding even though the latter may contribute to CNT/polymer interactions (e.g., Namilae and Chandra, 2005; Thostenson et al., 2005). The energy between two atoms of distance r due to van der Waals force is usually represented by the Lennard–Jones 6–12 potential,

$$V(r) = 4\varepsilon\left(\frac{\sigma^{12}}{r^{12}} - \frac{\sigma^{6}}{r^{6}}\right), \tag{1.1}$$

where $\sqrt[6]{2}\sigma$ is the equilibrium distance between the atoms, ε is the bond energy at the equilibrium distance, and they take the values $\varepsilon = 0.004656\,\text{eV}$ and $\varepsilon = 0.3825\,\text{nm}$ for carbon atoms of the CNT and the $-CH_2-$ units of polyethylene (Frankland et al., 2003). In Section 2.1, we establish a cohesive law for a graphene and polymer molecules based on the van der Waals force in (1.1). We extend such an approach to a CNT in an infinite polymer in Section 2.2. The effect of finite polymer boundary (e.g., traction-free surface) is studied in Section 3. These analytical cohesive laws are suitable for the study of CNT-reinforced polymer matrix composites. In Section 4, we derive the cohesive law for an arbitrary pair

potential which includes the Lennard–Jones 6–12 potential (1.1) as a special case. The effect of CNT and polymer surface waviness is discussed in Section 5.

2. The cohesive law for a carbon nanotube in an infinite polymer matrix

2.1. Graphene/polymer

We first neglect the effect of CNT radius and study the interaction between a graphene (i.e., an infinite plane of carbon atoms) and polymer. The graphene is parallel to the polymer surface, and h denotes their equilibrium distance (Fig. 1a). In order to establish a continuum cohesive law, we homogenize carbon atoms on the graphene and represent them by an area density ρ_c, where ρ_c is related to the equilibrium bond length l_0 of graphene prior to deformation by $\rho_c = 4/\left(3\sqrt{3}l_0^2\right)$. The effect of homogenization to represent discrete carbon atoms by the area density is discussed in Section 6. The number of carbon atoms over an area $\mathrm{d}A$ on the graphene is $\rho_c\,\mathrm{d}A$. Similarly, the volume density of polymer molecules is denoted by ρ_p, and the number of polymer molecules over a volume $\mathrm{d}V$ is $\rho_p\,\mathrm{dV}$.

The distance between a point (0,0) on the graphene and a point (x, z) $(x \leqslant -h, z \geqslant 0)$ in the polymer (Fig. 1a) is $r = \sqrt{x^2 + z^2}$. The energy due to the van der Waals force is given by $V(r)$ in (1.1). For an infinitesimal area $\mathrm{d}A$, the energy stored due to the van der Waals force is

$$\rho_c\,\mathrm{d}A \int_{V_{\text{polymer}}} V(r)\rho_p\,\mathrm{d}V_{\text{polymer}} = 2\pi\rho_p\rho_c\,\mathrm{d}A \int_{-\infty}^{-h} \mathrm{d}x \int_0^{\infty} V(r) z\,\mathrm{d}z. \tag{2.1}$$

The cohesive energy Φ is the energy per unit area, and is given by

$$\Phi = 2\pi\rho_p\rho_c \int_{-\infty}^{-h} \mathrm{d}x \int_0^{\infty} V(r) z\,\mathrm{d}z = \frac{2\pi}{3}\rho_p\rho_c\varepsilon\sigma^3\left(\frac{2\sigma^9}{15h^9} - \frac{\sigma^3}{h^3}\right), \tag{2.2}$$

where $\sqrt[6]{2}\sigma$ is the equilibrium distance in the van der Waals force and ε is the corresponding bond energy. The equilibrium distance h is determined by minimizing the energy, $\partial\Phi/\partial h = 0$, as

$$h = \left(\frac{2}{5}\right)^{1/6}\sigma = 0.858\sigma. \tag{2.3}$$

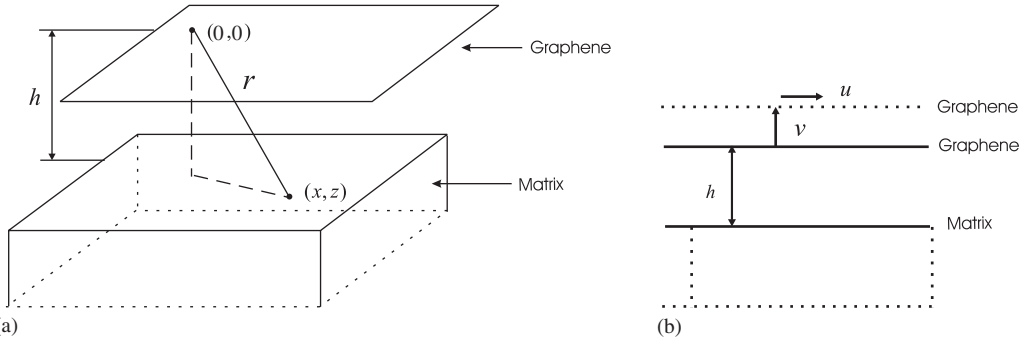

Fig. 1. A schematic diagram of a graphene parallel to the surface of an infinite polymer: (a) the distance between the graphene and polymer surface is h; (b) the graphene is subjected to the opening and sliding displacements.

For the opening displacement v and sliding displacement u beyond the equilibrium distance h, as shown in Fig. 1b, the cohesive energy can be similarly obtained as

$$\Phi = \frac{2\pi}{3}\rho_p\rho_c\varepsilon\sigma^3\left[\frac{2\sigma^9}{15(h+v)^9} - \frac{\sigma^3}{(h+v)^3}\right], \tag{2.4}$$

which can also be obtained from (2.2) by simply replacing h with $h+v$. Eq. (2.4) is independent of the sliding displacement u because sliding does not change the van der Waals force for infinite graphene and polymer. This leads to a vanishing shear cohesive stress

$$\tau_{\text{cohesive}} = \frac{\partial\Phi}{\partial u} = 0. \tag{2.5}$$

The tensile cohesive stress is obtained from (2.4) as

$$\sigma_{\text{cohesive}} = \frac{\partial\Phi}{\partial v} = 2\pi\rho_p\rho_c\varepsilon\sigma^2\left[\frac{\sigma^4}{(h+v)^4} - \frac{2\sigma^{10}}{5(h+v)^{10}}\right]. \tag{2.6}$$

Eqs. (2.5) and (2.6) give the cohesive law for graphene/polymer based on the van der Waals force. Such a cohesive law gives the following cohesive properties:

(1) initial slope $(\mathrm{d}\sigma_{\text{cohesive}}/\mathrm{d}v \text{ at } v=0) = 30\left(\frac{2}{5}\right)^{1/6}\pi\rho_p\rho_c\varepsilon\sigma$;
(2) cohesive strength (maximum cohesive stress) $\sigma_{\max} = \frac{6\pi}{5}\rho_p\rho_c\varepsilon\sigma^2$;
(3) critical separation $\delta_0 = \sigma - h = \left[1 - \left(\frac{2}{5}\right)^{1/6}\right]\sigma$ at which the cohesive strength is reached; and
(4) total cohesive energy (area underneath the $\sigma_{\text{cohesive}}\sim v$ curve) $\Phi_{\text{total}} = \frac{4\pi}{9}\sqrt{\frac{5}{2}}\rho_p\rho_c\varepsilon\sigma^3$.

The cohesive law in (2.4) and (2.6) can be rewritten in terms of the cohesive strength $\sigma_{\max}$ and total cohesive energy Φ_{total} as

$$\Phi = \frac{\Phi_{\text{total}}}{2}\left\{\frac{1}{\left[1+0.682\frac{\sigma_{\max}}{\Phi_{\text{total}}}v\right]^9} - \frac{3}{\left[1+0.682\frac{\sigma_{\max}}{\Phi_{\text{total}}}v\right]^3}\right\}, \tag{2.7}$$

$$\sigma_{\text{cohesive}} = 3.07\sigma_{\max}\left\{\frac{1}{\left[1+0.682\frac{\sigma_{\max}}{\Phi_{\text{total}}}v\right]^4} - \frac{1}{\left[1+0.682\frac{\sigma_{\max}}{\Phi_{\text{total}}}v\right]^{10}}\right\}. \tag{2.8}$$

The initial slope and critical separation are given in terms of $\sigma_{\max}$ and Φ_{total} by $12.6\,\sigma_{\max}^2/\Phi_{\text{total}}$ and $0.242\,\Phi_{\text{total}}/\sigma_{\max}$, respectively.

2.2. Carbon nanotube/polymer

We now account for the effect of CNT radius and study a CNT embedded in an infinite polymer matrix. Let h now denote the equilibrium distance between the CNT and polymer surface (Fig. 2). We homogenize carbon atoms on the CNT and represent them by an area density ρ_c (which may be slightly different from the area density of graphene due to the effect of CNT radius). The volume density of polymer molecules is still denoted by ρ_p.

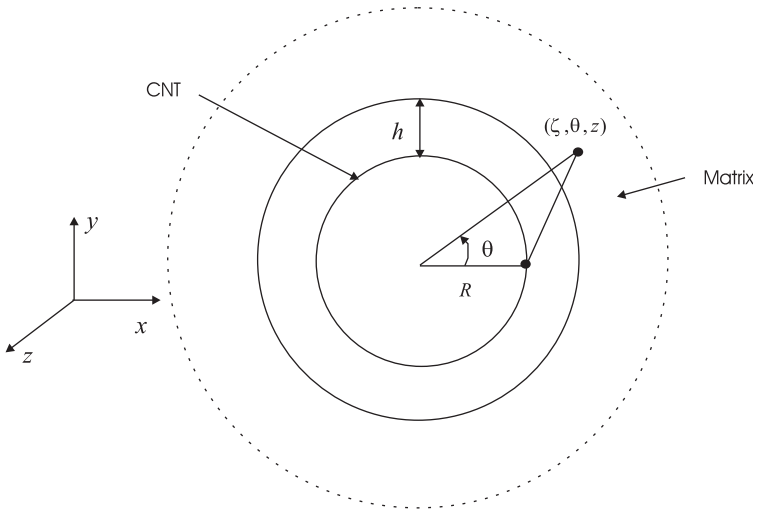

Fig. 2. A schematic diagram of a carbon nanotube (CNT) in a polymer matrix. The CNT radius is R, and the distance between the CNT and polymer surface is h.

The cylindrical coordinates (R, θ, z) are used, where z denotes the central axis of the CNT. Without losing generality, we take a point (R, 0, 0) on the CNT and a point (ζ, θ, z) ($\zeta \geqslant R+h$) in the polymer, where R is the CNT radius. The distance between these two points is $r = \sqrt{\zeta^2 - 2R\zeta\cos\theta + R^2 + z^2}$. The energy due to the van der Waals force is still given by $V(r)$ in (1.1).

We examine a section of CNT and polymer with height $\mathrm{d}z$. The energy stored in this section due to the van der Waals force is

$$\rho_c 2\pi R\,\mathrm{d}z \int_{V_{\text{polymer}}} V(r)\rho_p\,\mathrm{d}V_{\text{polymer}} = 2\pi\rho_p\rho_c R\,\mathrm{d}z \int_{R+h}^{\infty} \zeta\,\mathrm{d}\zeta \int_0^{2\pi} \mathrm{d}\theta \int_{-\infty}^{\infty} V(r)\mathrm{d}z', \quad (2.9)$$

where $r = \sqrt{\zeta^2 - 2R\zeta\cos\theta + R^2 + z'^2}$. The cohesive energy Φ is the energy per unit area, and is given by

$$\Phi = \frac{2\pi\rho_p\rho_c R\,\mathrm{d}z \int_{R+h}^{\infty} \zeta\,\mathrm{d}\zeta \int_0^{2\pi} \mathrm{d}\theta \int_{-\infty}^{\infty} V(r)\,\mathrm{d}z'}{2\pi\left(R+\frac{h}{2}\right)\mathrm{d}z} = \frac{\rho_p\rho_c R \int_{R+h}^{\infty} \zeta\,\mathrm{d}\zeta \int_0^{2\pi} \mathrm{d}\theta \int_{-\infty}^{\infty} V(r)\,\mathrm{d}z'}{R+\frac{h}{2}}, \quad (2.10)$$

where $2\pi(R+h/2)\mathrm{d}z$ is the average of CNT area $2\pi R\,\mathrm{d}z$ and polymer surface area $2\pi(R+h)\,\mathrm{d}z$. The above triple integral can be simplified to a single integral in Appendix A.

Fig. 3 shows the cohesive energy, normalized by the total cohesive energy for graphene $\Phi_{\text{total}} = \frac{4\pi}{9}\sqrt{\frac{5}{2}}\rho_p\rho_c\varepsilon\sigma^3$, versus the distance h between the CNT and polymer surface for several CNT radii, where h is normalized by its equilibrium value $\left(\frac{2}{5}\right)^{1/6}\sigma$ in (2.3) for graphene, and $\sigma = 0.3825\,\text{nm}$ is the characteristic length in the van der Waals force. The curves for different CNTs are very close, and they are all close to that for graphene. This suggests that the CNT radius has little effect on the cohesive energy. Each curve has a

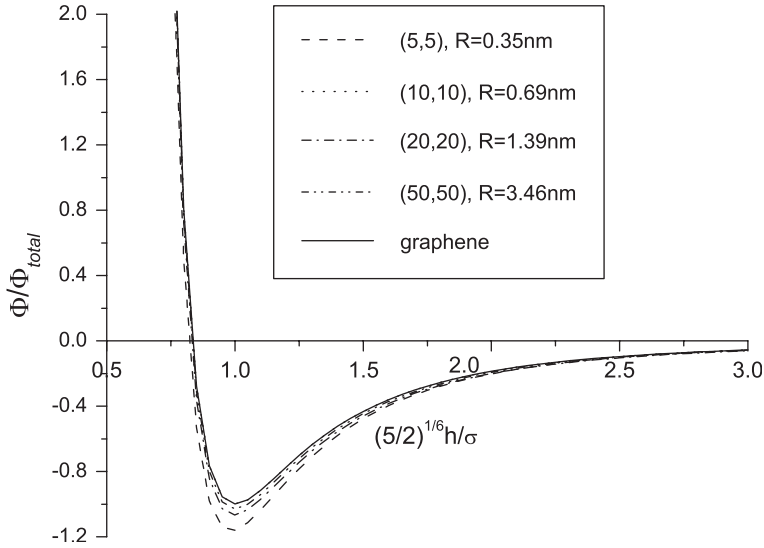

Fig. 3. The cohesive energy, normalized by the total cohesive energy Φ_{total} for graphene, versus the distance h between the carbon nanotube (CNT) and polymer surface for several CNT radii and graphene, where h is normalized by its equilibrium value $\left(\frac{2}{5}\right)^{1/6}\sigma$ for graphehe, and $\sigma = 0.3825\,\text{nm}$ is the characteristic length in the van der Waals force.

minimum, corresponding to the equilibrium distance between the CNT and polymer surface, and this distance is very close to $\left(\frac{2}{5}\right)^{1/6}\sigma$.

Similar to graphene, the cohesive energy for a CNT in an infinite polymer matrix is independent of the sliding displacement u such that the shear cohesive stress vanishes. Since the effect of CNT radius is small as shown in Fig. 3, the cohesive energy and tensile cohesive stress are still given approximately by (2.4) and (2.6), respectively, and the cohesive law in (2.7) and (2.8) also holds. Fig. 4 shows the tensile cohesive stress σ_{cohesive}, normalized by the cohesive strength $\sigma_{\max}$, versus the normalized opening displacement v/δ_0, where $\delta_0 = 0.242\,\Phi_{\text{total}}/\sigma_{\max}$ is the critical separation at which the cohesive strength is reached, and $\delta_0 = 0.0542\,\text{nm}$ for CNTs/polyethylene. The cohesive stress increases rapidly at small opening displacement, and gradually decreases after the cohesive strength is reached.

3. The cohesive law for a carbon nanotube in a finite polymer matrix

We first study the interaction between a graphene and polymer that overlap over a length L, as shown in Fig. 5. The distance between the graphene and polymer surface is h. The area density of the graphene and volume density of polymer molecules are ρ_{c} and ρ_{p}, respectively.

Fig. 5 shows the Cartesian coordinates (x, y, z), where x is the direction normal to the graphene (and polymer surface), and y is along the graphene free edge. The graphene free edge is represented by $(0, y, 0)$ while the free edge of polymer surface is $(-h, y, L)$. Without losing generality we consider a point $(0, 0, z_{\text{c}})$ $(z_{\text{c}} \geqslant 0)$ on the graphene, and a point (x, y, z_{p})

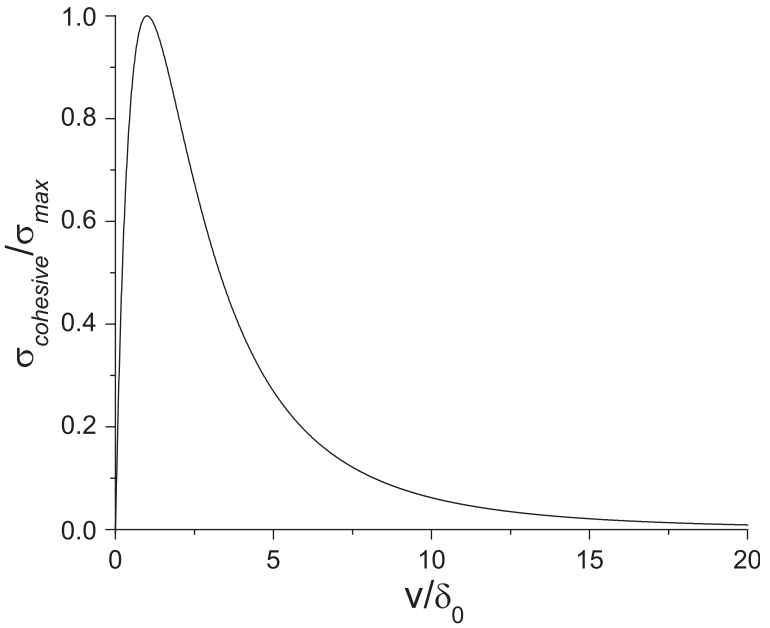

Fig. 4. The tensile cohesive stress σ_{cohesive}, normalized by the cohesive strength $\sigma_{\max}$, versus the normalized opening displacement v/δ_0, where $\delta_0 = 0.242\,\Phi_{\text{total}}/\sigma_{\max}$ is the critical separation at which the cohesive strength is reached, and $\delta_0 = 0.0542\,\text{nm}$ for carbon nanotubes/polyethylene.

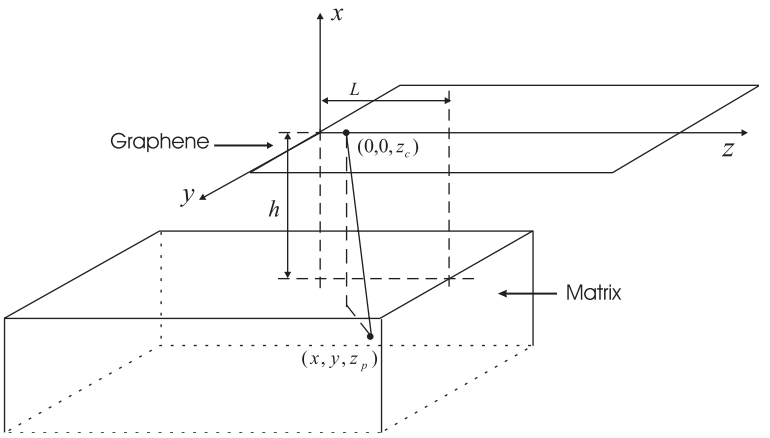

Fig. 5. A schematic diagram of a graphene parallel to the surface of a semi-infinite polymer; the graphene/polymer overlap length is L, and the distance between the graphene and polymer surface is h.

($x \leqslant -h,\ z_p \leqslant L$) in the polymer (Fig. 5). The distance between these two points is $r = \sqrt{x^2 + y^2 + (z_{\text{p}} - z_{\text{c}})^2}$. The energy due to van der Waals force is given by $V(r)$ in (1.1).

Unlike the analysis in Section 2, the deformation for finite graphene and polymer is non-uniform. We define the energy per unit thickness Φ_{line} (along the free edge) stored due to

van der Waals forces as

$$\begin{aligned}\Phi_{\text{line}} &= \int_0^{\infty} \rho_{\text{c}}\,\mathrm{d}z_{\text{c}} \int_{V_{\text{polymer}}} V(r)\rho_{\text{p}}\,\mathrm{d}V_{\text{polymer}} \\ &= \rho_{\text{p}}\rho_{\text{c}} \int_0^{\infty} \mathrm{d}z_{\text{c}} \int_{-\infty}^{-h} \mathrm{d}x \int_{-\infty}^{\infty} \mathrm{d}y \int_{-\infty}^{L} V(r)\,\mathrm{d}z_{\text{p}},\end{aligned} \tag{3.1}$$

which can be integrated analytically to give

$$\Phi_{\text{line}} = \frac{2\pi}{3}\rho_{\text{p}}\rho_{\text{c}}\varepsilon\sigma^3 \left\{ \frac{\sigma^9}{15h^9} \left[\begin{array}{c} L\left(1+\frac{h^9}{8L^9}\right) + \sqrt{h^2+L^2}\left(1+\frac{5h^2}{128L^2} - \frac{3h^4}{64L^4} + \frac{h^6}{16L^6} - \frac{h^8}{8L^8}\right) \\ - \frac{69h^2}{128\sqrt{h^2+L^2}} - \frac{15h^4}{128\sqrt{\left(h^2+L^2\right)^3}} - \frac{9h^6}{128\sqrt{\left(h^2+L^2\right)^5}} \end{array} \right] \right. \\ \left. - \frac{\sigma^3}{2h^3}\left[L\left(1+\frac{h^3}{2L^3}\right) + \sqrt{h^2+L^2}\left(1-\frac{h^2}{2L^2}\right)\right] \right\}. \tag{3.2}$$

For the overlap length L (Fig. 5) larger than h, the Taylor expansion of (3.2) with respect to h/L gives

$$\Phi_{\text{line}}(L,h) = \frac{2\pi}{3}\rho_{\text{p}}\rho_{\text{c}}\varepsilon\sigma^3\left(\frac{2\sigma^9}{15h^9} - \frac{\sigma^3}{h^3}\right)L\left[1+O\left(\frac{h^3}{L^3}\right)\right], \tag{3.3}$$

where $\frac{2\pi}{3}\rho_{\text{p}}\rho_{\text{c}}\varepsilon\sigma^3\left(\frac{2\sigma^9}{15h^9} - \frac{\sigma^3}{h^3}\right)$ is identical to (2.2) for infinite graphene and polymer matrix; the terms neglected are on the order of h^3/L^3, and therefore are very small. The equilibrium distance h determined from $\partial\Phi_{\text{line}}/\partial h = 0$ is

$$h = 0.858\sigma\left[1+O\left(\frac{\sigma^3}{L^3}\right)\right], \tag{3.4}$$

which is essentially the same as (2.3) for infinite graphene and polymer. Fig. 6 compares the energy Φ_{line} given by the exact solution (3.2) and approximate solution (3.3), where Φ_{line} is normalized by $\Phi_{\text{total}}h$, and the equilibrium distance h is taken as 0.858σ. For length $L > h$, (3.3) is an excellent approximation of the exact solution (3.2).

For the opening displacement v and sliding displacement u beyond the equilibrium distance h, Φ_{line} is obtained from (3.2) by replacing L and h with $L-u$ and $h+v$, respectively, i.e.,

$$\Phi_{\text{line}} = \Phi_{\text{line}}(L-u, h+v). \tag{3.5}$$

It depends on the sliding and opening displacements through the current overlap length $L-u$ and distance $h+v$ between the graphene and polymer surface. For $L-u \gg h+v$, the Taylor expansion in (3.3) becomes

$$\Phi_{\text{line}}(L,h) = \frac{2\pi}{3}\rho_{\text{p}}\rho_{\text{c}}\varepsilon\sigma^3\left[\frac{2\sigma^9}{15(0.858\sigma+v)^9} - \frac{\sigma^3}{(0.858\sigma+v)^3}\right](L-u), \tag{3.6}$$

where h has been replaced by 0.858σ.

The tangential and normal forces (per unit thickness along the graphene free edge) are

$$F_{\text{tangent}} = \frac{\partial\Phi_{\text{line}}}{\partial u} \approx \frac{2\pi}{3}\rho_{\text{p}}\rho_{\text{c}}\varepsilon\sigma^3\left[\frac{\sigma^3}{(0.858\sigma+v)^3} - \frac{2\sigma^9}{15(0.858\sigma+v)^9}\right], \tag{3.7}$$

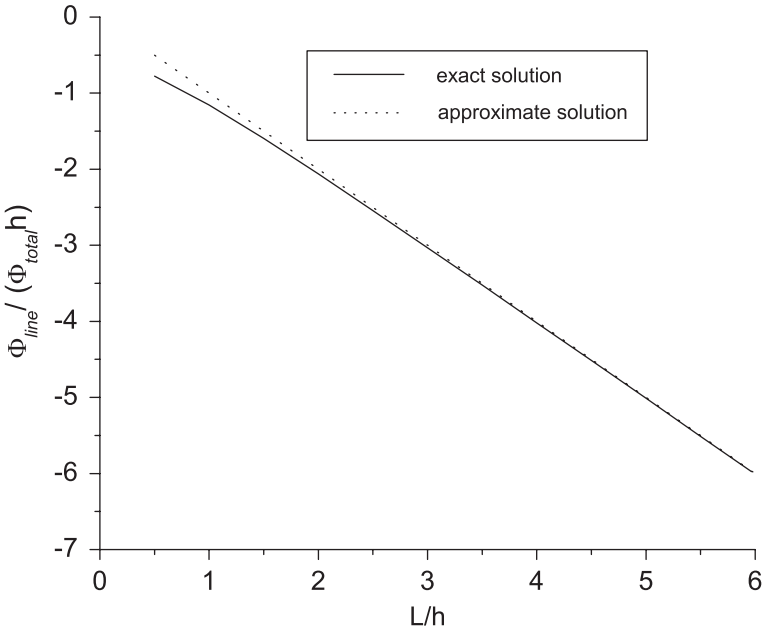

Fig. 6. The energy Φ_{line}, normalized by $\Phi_{\text{total}}h$, versus the normalized overlap length L/h, where Φ_{total} is the total cohesive energy for graphene and h is the distance between graphene and polymer surface.

$$F_{\text{normal}} = \frac{\partial \Phi_{\text{line}}}{\partial v} \approx 2\pi\rho_{\text{p}}\rho_{\text{c}}\varepsilon\sigma^2\left[\frac{\sigma^4}{(0.858\sigma+v)^4} - \frac{2\sigma^{10}}{5(0.858\sigma+v)^{10}}\right](L-u). \tag{3.8}$$

We define the average shear and tensile cohesive stresses over the current overlap length $L-u$ as

$$\tau_{\text{cohesive}} = \frac{F_{\text{tangent}}}{L-u} \approx \frac{2\pi}{3}\rho_{\text{p}}\rho_{\text{c}}\varepsilon\sigma^2\left[\frac{\sigma^3}{(0.858\sigma+v)^3} - \frac{2\sigma^9}{15(0.858\sigma+v)^9}\right]\frac{\sigma}{L-u}, \tag{3.9}$$

$$\sigma_{\text{cohesive}} = \frac{F_{\text{normal}}}{L-u} \approx 2\pi\rho_{\text{p}}\rho_{\text{c}}\varepsilon\sigma^2\left[\frac{\sigma^4}{(0.858\sigma+v)^4} - \frac{2\sigma^{10}}{5(0.858\sigma+v)^{10}}\right], \tag{3.10}$$

where the terms neglected are on the order of $\left(\sigma/(L-u)\right)^3$.

Eqs. (3.9) and (3.10) give the cohesive law for a finite graphene/polymer based on the van der Waals force. The average tensile cohesive stress σ_{cohesive} is identical to (2.6) for an infinite graphene/polymer, and does not depend on the sliding displacement u. Therefore the tensile cohesive law (2.8) given in terms of the cohesive strength $\sigma_{\max}$ and total cohesive energy Φ_{total} still holds. The average shear cohesive stress τ_{cohesive} in (3.9) is much smaller than σ_{cohesive} because $L-u \gg \sigma$, and it depends on both sliding and opening displacements, u and v, i.e., tension/shear coupling in the cohesive law. The shear cohesive law (3.9) can be rewritten in terms of the cohesive strength $\sigma_{\max}$ and total cohesive energy Φ_{total} as

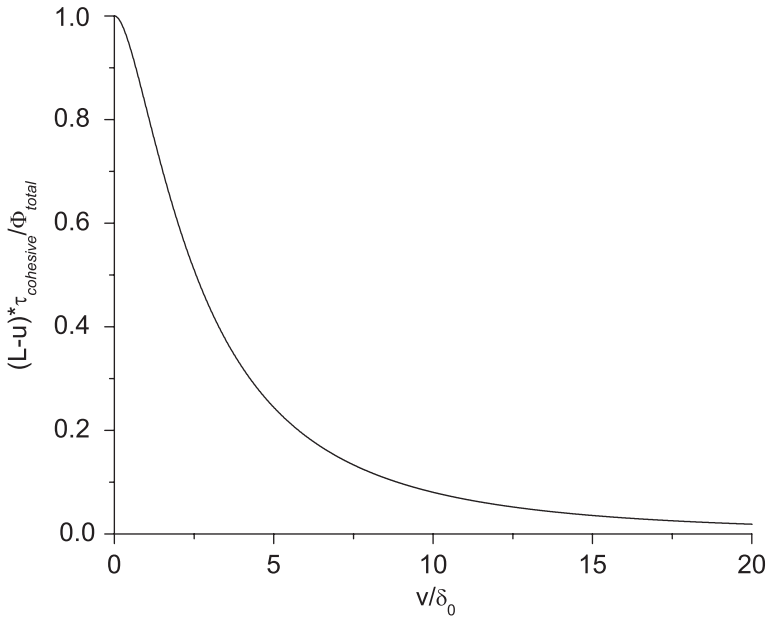

Fig. 7. The average shear cohesive stress τ_{cohesive}, normalized by the current overlap length $L-u$ and total cohesive energy Φ_{total}, versus the normalized opening displacement v/δ_0, where $\delta_0 = 0.242\,\Phi_{\text{total}}/\sigma_{\max}$ is the critical separation at which the tensile cohesive strength is reached, and $\delta_0 = 0.0542$ nm for CNTs/polyethylene.

$$\tau_{\text{cohesive}} = \frac{\sigma_{\max}}{2}\left\{\frac{3}{\left[1+0.682\frac{\sigma_{\max}}{\Phi_{\text{total}}}v\right]^3} - \frac{1}{\left[1+0.682\frac{\sigma_{\max}}{\Phi_{\text{total}}}v\right]^9}\right\}\frac{\Phi_{\text{total}}}{\sigma_{\max}(L-u)}. \tag{3.11}$$

Fig. 7 shows the average shear cohesive stress τ_{cohesive} normalized by the current overlap length $L-u$ and total cohesive energy Φ_{total}, $(L-u)\tau_{\text{cohesive}}/\Phi_{\text{total}}$, versus the normalized opening displacement v/δ_0, where $\delta_0 = 0.242\,\Phi_{\text{total}}/\sigma_{\max}$ is the critical separation at which the tensile cohesive strength is reached, and $\delta_0 = 0.0542$ nm for CNTs/polyethylene. The average shear cohesive stress is not zero even at $v = 0$, because the two sides of the overlap length L are not symmetric such that the tangential force does not vanish. In fact, at $v = 0$ τ_{cohesive} has a zero slope and a maximum $\Phi_{\text{total}}/(L-u)$, which is much smaller than $\sigma_{\max}$, and τ_{cohesive} decreases monotonically as v increases.

Similar to Section 2.2, the effect of CNT radius is small such that the analytical expressions of the cohesive law for graphene/polymer can be effectively used for CNT/polymer.

4. The cohesive law for an arbitrary pair potential

In this section, we extend the cohesive laws in Sections 2 and 3 for an arbitrary pair potential $V(r)$, which includes the Lennard–Jones 6–12 potential (1.1) as a special case. For an *infinite* matrix as in Section 2, the cohesive energy in (2.2) or (2.10) for an arbitrary pair potential $V(r)$ becomes

$$\Phi = 2\pi\rho_{\mathrm{p}}\rho_{\mathrm{c}}\int_{-\infty}^{-h}\mathrm{d}x\int_{0}^{\infty}V(r)z\,\mathrm{d}z = 2\pi\rho_{\mathrm{p}}\rho_{\mathrm{c}}\int_{h}^{\infty}V(r)r(r-h)\,\mathrm{d}r, \tag{4.1}$$

where $r=\sqrt{x^2+z^2}$, and we have exchanged the order of integrations to give the single integral in (4.1). The equilibrium distance h is determined from energy minimization $\partial\Phi/\partial h=0$, which gives $\int_h^\infty V(r)r\,\mathrm{d}r=0$. For the opening displacement v beyond the equilibrium distance h, the cohesive energy is obtained by simply replacing h with $h+v$,

$$\Phi = 2\pi\rho_{\mathrm{p}}\rho_{\mathrm{c}}\int_{h+v}^{\infty}V(r)r(r-h-v)\,\mathrm{d}r, \tag{4.2}$$

which gives vanishing shear cohesive stress $\tau_{\mathrm{cohesive}}=\partial\Phi/\partial u=0$ and a finite tensile cohesive stress

$$\sigma_{\mathrm{cohesive}} = \frac{\partial\Phi}{\partial v} = -2\pi\rho_{\mathrm{p}}\rho_{\mathrm{c}}\int_{h+v}^{\infty}V(r)r\,\mathrm{d}r. \tag{4.3}$$

Eqs. (4.2) and (4.3) give the cohesive law for an arbitrary pair potential $V(r)$.

For a *finite* matrix with the overlap length L as in Section 3, the energy per unit thickness $\Phi_{\mathrm{line}}=\rho_{\mathrm{p}}\rho_{\mathrm{c}}\int_0^\infty\mathrm{d}z_{\mathrm{c}}\int_{-\infty}^{-h}\mathrm{d}x\int_{-\infty}^{\infty}\mathrm{d}y\int_{-\infty}^{L}V\left[\sqrt{x^2+y^2+\left(z_{\mathrm{p}}-z_{\mathrm{c}}\right)^2}\right]\mathrm{d}z_{\mathrm{p}}$ in (3.1) can be re-written via the change of integration variables $\xi=z_{\mathrm{p}}-z_{\mathrm{c}}$ and $\eta=z_{\mathrm{p}}+z_{\mathrm{c}}$ as

$$\Phi_{\mathrm{line}} = \rho_{\mathrm{p}}\rho_{\mathrm{c}}\int_{-\infty}^{-h}\mathrm{d}x\int_{-\infty}^{\infty}\mathrm{d}y\int_{-\infty}^{L}(L-\xi)V\left(\sqrt{x^2+y^2+\xi^2}\right)\mathrm{d}\xi. \tag{4.4}$$

By further change of integration variables $r=\sqrt{x^2+y^2+\xi^2}$ and $\theta=\tan^{-1}y/x$, (4.4) can be expressed as

$$\Phi_{\mathrm{line}} = 2\rho_{\mathrm{p}}\rho_{\mathrm{c}}\int_{h}^{\infty}V(r)r\ f(r,h,L)\,\mathrm{d}r, \tag{4.5}$$

where

$$f(r,h,L)=\int_{-\sqrt{r^2-h^2}}^{\min\left(\sqrt{r^2-h^2},L\right)}(L-\xi)\cos^{-1}\frac{h}{\sqrt{r^2-\xi^2}}\mathrm{d}\xi,$$

and min stands for the minimum between two variables. For $L\gg h$, $f(r,h,L)$ approaches $\pi(r-h)L$ such that (4.5) becomes

$$\Phi_{\mathrm{line}} \approx 2\pi\rho_{\mathrm{p}}\rho_{\mathrm{c}}\int_{h}^{\infty}V(r)r(r-h)\,\mathrm{d}r\ \ L, \tag{4.6}$$

where $2\pi\rho_{\mathrm{p}}\rho_{\mathrm{c}}\int_h^\infty V(r)r(r-h)\,\mathrm{d}r$ is identical to (4.1). For the opening displacement v and sliding displacement u beyond the equilibrium distance h, Φ_{line} is obtained from (4.6) by simply replacing L and h with $L-u$ and $h+v$, respectively,

$$\Phi_{\mathrm{line}} \approx 2\pi\rho_{\mathrm{p}}\rho_{\mathrm{c}}\int_{h+v}^{\infty}V(r)r(r-h-v)\,\mathrm{d}r(L-u). \tag{4.7}$$

The tangential and normal forces (per unit thickness along the graphene free edge) are $F_{\mathrm{tangent}}=\frac{\partial\Phi_{\mathrm{line}}}{\partial u}\approx-2\pi\rho_{\mathrm{p}}\rho_{\mathrm{c}}\int_{h+v}^{\infty}V(r)r(r-h-v)\,\mathrm{d}r$ and $F_{\mathrm{normal}}=\frac{\partial\Phi_{\mathrm{line}}}{\partial v}\approx-2\pi\rho_{\mathrm{p}}\rho_{\mathrm{c}}\int_{h+v}^{\infty}V(r)r\,\mathrm{d}r(L-u)$. The average shear cohesive stress over the current overlap length

$L-u$ is

$$\tau_{\text{cohesive}} \approx -\frac{2\pi\rho_{\text{p}}\rho_{\text{c}}}{L-u}\int_{h+v}^{\infty} V(r)r(r-h-v)\,\mathrm{d}r. \tag{4.8}$$

The average tensile cohesive stress is the same as (4.3). Eqs. (4.3) and (4.8) give the cohesive law for a finite matrix based on an arbitrary pair potential $V(r)$.

5. Polymer surface roughness

The polymer surface is assumed to be flat in Sections 2–4, which neglects the polymer surface roughness. Polymer of chain molecules exhibits irregular surface structure and roughness (e.g., Lordi and Yao, 2000; Frankland et al., 2002, 2003; Rapaport, 2004). We use the simple model shown in Fig. 8 to estimate the effect of polymer surface roughness on the cohesive law. The polymer surface is wavy in z direction, and has an amplitude Δ and wavelength λ. The average distance between the polymer surface and graphene is still denoted by h. Let x be the coordinate along the normal direction of the graphene. The distance between a point $(0, 0, z_{\text{c}})$ on the graphene and a point (x, y, z_{p}) in the polymer (Fig. 8) is $r=\sqrt{x^2+y^2+\left(z_{\text{p}}-z_{\text{c}}\right)^2}$, where $x \leqslant -h-\Delta\cos\left(\frac{2\pi z_{\text{p}}}{\lambda}\right)$. The average cohesive energy for an arbitrary pair potential $V(r)$ is given by

$$\begin{aligned}\Phi &= \rho_{\text{p}}\rho_{\text{c}}\frac{1}{\lambda}\int_{-\lambda/2}^{\lambda/2}\mathrm{d}z_{\text{c}}\int_{V_{\text{polymer}}} V(r)\,\mathrm{d}V_{\text{polymer}} \\ &= \frac{\rho_{\text{p}}\rho_{\text{c}}}{\lambda}\int_{-\lambda/2}^{\lambda/2}\mathrm{d}z_{\text{c}}\int_{-\infty}^{\infty}\mathrm{d}y\int_{-\infty}^{\infty}\mathrm{d}z_{\text{p}}\int_{-\infty}^{-h-\Delta\cos\frac{2\pi z_{\text{p}}}{\lambda}} V\left[\sqrt{x^2+y^2+\left(z_{\text{p}}-z_{\text{c}}\right)^2}\right]\mathrm{d}x,\end{aligned} \tag{5.1}$$

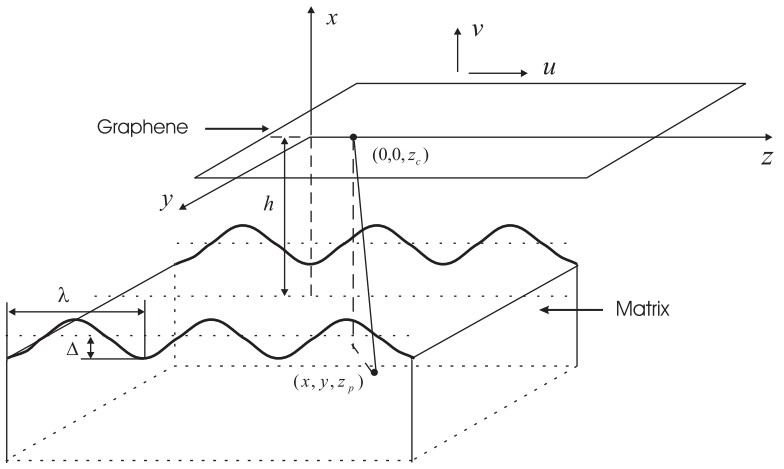

Fig. 8. A schematic diagram of a graphene on a wavy polymer surface that has the amplitude Δ and wavelength λ. The average distance between the graphene and polymer surface is denoted by h. The graphene is subjected to the opening and sliding displacements.

where $\frac{1}{\lambda}\int_{-\lambda/2}^{\lambda/2} \mathrm{d}z_c$ represents the average over the wavelength λ. For the opening displacement v and sliding displacement u (along the wavy direction x) as shown in Fig. 8, the cohesive energy can be similarly obtained by replacing x with $x - v$ and $z_p - z_c$ with $z_p - z_c - u$, respectively

$$\Phi = \frac{\rho_p \rho_c}{\lambda}\int_{-\lambda/2}^{\lambda/2} \mathrm{d}z_c \int_{-\infty}^{\infty} \mathrm{d}y \int_{-\infty}^{\infty} \mathrm{d}z_p \int_{-\infty}^{-h-\Delta\cos\frac{2\pi z_p}{\lambda}} V\left[\sqrt{(x-v)^2 + y^2 + \left(z_p - z_c - u\right)^2}\right] \mathrm{d}x$$
$$= \frac{\rho_p \rho_c}{\lambda}\int_{-\lambda/2}^{\lambda/2} \mathrm{d}z_c \int_{-\infty}^{\infty} \mathrm{d}y \int_{-\infty}^{\infty} \mathrm{d}z' \int_{-\infty}^{-h-v-\Delta\cos\frac{2\pi(z'+z_c+u)}{\lambda}} V\left(\sqrt{x'^2 + y^2 + z'^2}\right) \mathrm{d}x', \quad (5.2)$$

where the integration variables have been changed to $z' = z_p - z_c - u$ and $x' = x - v$. The shear cohesive stress is given by $\tau_{\text{cohesive}} = \frac{\partial \Phi}{\partial u} = 2\pi\Delta\frac{\rho_p\rho_c}{\lambda^2}\int_{-\lambda/2}^{\lambda/2}\mathrm{d}z_c\int_{-\infty}^{\infty}\mathrm{d}y$ $\int_{-\infty}^{\infty} V(r')\sin\frac{2\pi(z'+z_c+u)}{\lambda}\,\mathrm{d}z'$, where $r' = \sqrt{\left[h+v+\Delta\cos\frac{2\pi(z'+z_c+u)}{\lambda}\right]^2 + y^2 + z'^2}$. This integral can be evaluated analytically to give

$$\tau_{\text{cohesive}} = 0, \quad (5.3)$$

i.e., the shear cohesive stress vanishes for a wavy polymer surface and flat graphene. In fact, such a conclusion of *vanishing shear cohesive stress* also holds for

(1) *an arbitrary* periodic *polymer surface and flat graphene*, *and*
(2) *an arbitrary polymer surface and wavy graphene that have the* same period.

The tensile cohesive stresses is given by $\sigma_{\text{cohesive}} = \frac{\partial \Phi}{\partial v} = -\frac{\rho_p\rho_c}{\lambda}\int_{-\lambda/2}^{\lambda/2}\mathrm{d}z_c\int_{-\infty}^{\infty}\mathrm{d}y\int_{-\infty}^{\infty}V(r')\,\mathrm{d}z'$, where r' is given above. This integral can also be evaluated analytically to give

$$\sigma_{\text{cohesive}} = -2\pi\rho_p\rho_c\left[\int_{h+v-\Delta}^{\infty} V(r) r\,\mathrm{d}r - \frac{1}{\pi}\int_{h+v-\Delta}^{h+v+\Delta} V(r) r\cos^{-1}\frac{r-h-v}{\Delta}\,\mathrm{d}r\right]. \quad (5.4)$$

Since the amplitude Δ of polymer wavy surface must be less than $h + v$ (otherwise the polymer surface penetrates the graphene), the Taylor expansion of (5.4) with respect to Δ gives

$$\sigma_{\text{cohesive}} = -2\pi\rho_p\rho_c\int_{h+v}^{\infty} V(r) r\,\mathrm{d}r + \frac{\pi}{2}\rho_p\rho_c[V(h+v) + (h+v)V'(h+v)]\Delta^2 + O(\Delta^3). \quad (5.5)$$

Its difference with the tensile cohesive stress in (4.3) for a flat polymer surface is on the order of Δ^2.

6. Concluding remarks and discussion

We have obtained the cohesive law for the carbon nanotubes/polymer interfaces based on the van der Waals force. The cohesive law is governed by two parameters, namely the tensile cohesive strength $\sigma_{\max}$ and cohesive energy Φ_{total} which are given in terms of the area density of carbon nanotubes and volume density of polymer, as well as the parameters in the van der Waals force. For a CNT in an infinite polymer, the shear cohesive stress

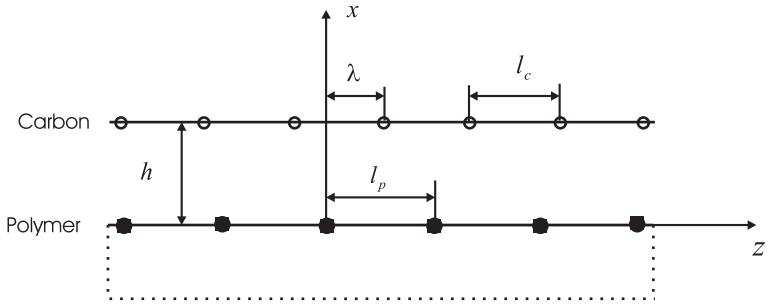

Fig. 9. A simple one-dimensional model of carbon atoms and polymer molecules interacting via the van der Waals force.

τ_{cohesive} vanishes, and the tensile cohesive stress σ_{cohesive} depends only on the opening displacement v. For a CNT in a finite polymer matrix, σ_{cohesive} remains the same, but τ_{cohesive} depends on both opening displacement v and sliding displacement u, i.e., the tension/shear coupling. The simple, analytical expressions of the cohesive law are useful to study the interaction between CNTs and polymer, such as in CNT-reinforced composites. The effect of polymer surface waviness on the interface cohesive law is also studied. The above approach can also be applied to other not well-bonded interfaces for which the van der Waals force is the dominating mechanism of interaction.

The present analysis involves several approximations. First, the carbon atoms and polymer molecules are homogenized and represented by the area and volume densities in Sections 2–4. We have developed a simple model shown in Fig. 9 and Appendix B to demonstrate that such an approximation indeed captures the average behavior of CNT/polymer interfaces.

Another approximation is to neglect any chemical bonding between CNTs and polymer. Even though CNTs are generally not well bonded to polymer, small amount of chemical bonding may contribute to the interface strength, particularly the shear resistance against interface sliding.

Acknowledgements

LYJ was supported by a Postdoctoral Fellowship from the Natural Sciences and Engineering Research Council of Canada (NSERC) and by Canadian Space Agency. This research was also supported by ONR Composites for Marine Structures Program (grant N00014-01-1-0205, Program Manager Dr. Y. D. S. Rajapakse), NSF and NSFC.

Appendix A

Eq. (2.10) can be expressed as

$$\Phi = \pi\rho_{\text{p}}\rho_{\text{c}}\varepsilon\sigma^3 \frac{R}{2R+h}\int_0^{2\pi}\left(\sigma^9\varphi_9 - \sigma^3\varphi_3\right)\mathrm{d}\theta, \tag{A.1}$$

where

$$\varphi_9 = \frac{7}{32R_h^9} + \frac{R\cos\theta}{R_h^9\left(R_h + R_h'\right)^5}\left(\frac{4}{5}R_h^4 + \frac{65}{32}R_h^3R_h' + \frac{69}{32}R_h^2R_h'^2 + \frac{35}{32}R_hR_h'^3 + \frac{7}{32}R_h'^4\right),$$

$$\varphi_3 = \frac{1}{R_h^3} + \frac{R\cos\theta}{R_h^3\left(R_h + R_h'\right)^2}\left(2R_h + R_h'\right), \quad R_h = \sqrt{(R+h)^2 + R^2 - 2R(R+h)\cos\theta},$$

and $R_h' = R + h - R\cos\theta$.

Appendix B

For simplicity we use the one-dimensional model in Fig. 9, but the approach also holds for two- and three-dimensional analyses. Let h denote the equilibrium distance between two planes, and l_c and l_p the spacing between carbon atoms and between polymer molecules, respectively. The distance between each carbon atom and a representative polymer molecule (sitting at the origin, Fig. 9) is $r_n = \sqrt{h^2 + (\lambda + nl_c)^2}$, where $n = 0, \pm1, \pm2, \pm3, \ldots$ represent all carbon atoms, λ is the projected distance on the plane between the representative polymer molecule and nearby carbon atom (Fig. 9), and it is a random number between 0 and l_c since carbon atoms and polymer molecules do not form bonds and interact only through the van der Waals force. The energy of the representative polymer molecule is $\frac{1}{2}\sum_{n=-\infty}^{\infty} V(r_n)$. Its average (with respect to λ) is $\frac{1}{l_c}\int_0^{l_c}\frac{1}{2}\sum_{n=-\infty}^{\infty} V(r_n)\,\mathrm{d}\lambda$, which becomes $\frac{1}{2l_c}\sum_{n=-\infty}^{\infty}\int_{nl_c}^{(n+1)l_c} V\left(\sqrt{h^2+\lambda'^2}\right)\mathrm{d}\lambda' = \frac{1}{2l_c}\int_{-\infty}^{\infty} V\left(\sqrt{h^2+\lambda'^2}\right)\mathrm{d}\lambda'$ after the change of integration variable to $\lambda' = \lambda + nl_c$. The ratio of this average energy to the spacing l_p between polymer molecules gives the average energy in polymer per unit length (for this one-dimensional model) as $\frac{1}{2l_pl_c}\int_{-\infty}^{\infty} V\left(\sqrt{h^2+\lambda'^2}\right)\mathrm{d}\lambda'$. Similarly, it can be shown that the average energy in carbon per unit length is the same such that the cohesive energy is

$$\Phi = \frac{1}{l_pl_c}\int_{-\infty}^{\infty} V\left(\sqrt{h^2+\lambda'^2}\right)\mathrm{d}\lambda'. \tag{B.1}$$

It is identical to the results obtained by homogenizing the carbon atoms and polymer molecules first and then representing them by the length densities (for this one-dimensional model) $\rho_c = 1/l_c$ and $\rho_p = 1/l_p$.

References

Ajayan, P.M., Schadler, L.S., Giannaris, C., Rubio, A., 2000. Single-walled carbon nanotube-polymer composites: strength and weakness. Adv. Mater. 12, 750–753.

Bazant, Z.P., 2002. Concrete fracture models: testing and practice. Eng. Fract. Mech. 69 (2), 165–205.

Breuer, O., Sundararaj, U., 2004. Big returns from small fibers: a review of polymer/carbon nanotube composites. Polym. Compos. 25, 630–645.

Camacho, G.T., Ortiz, M., 1996. Computational modelling of impact damage in brittle materials. Int. J. Solids Struct. 33, 2899–2938.

Deepak, S., Wei, C., Cho, K., 2003. Nanomechanics of carbon nanotubes and composites. Appl. Mech. Rev. 56 (2), 215–230.

Elices, M., Guinea, G.V., Gomez, J., Planas, J., 2002. The cohesive zone model: advantages, limitations and challenges. Eng. Fract. Mech. 69 (2), 137–163.

Frankland, S.J.V., Caglar, A., Brenner, D.W., Griebel, M., 2002. Molecular simulation of the influence of chemical cross-links on the shear strength of carbon nanotube-polymer interfaces. J. Phys. Chem. B 106, 3046–3048.

Frankland, S.J.V., Harik, V.M., Odegard, G.M., Brenner, D.W., Gates, T.S., 2003. The stress–strain behavior of polymer-nanotube composites from molecular dynamics simulation. Compos. Sci. Technol. 63, 1655–1661.

Geubelle, P.H., Baylor, J.S., 1998. Impact-induced delamination of composites: a 2D simulation. Compos. B 29, 589–602.

Gou, J., Minaie, B., Wang, B., Liang, Z., Zhang, C., 2004. Computational and experimental study of interfacial bonding of single-walled nanotube reinforced composites. Comp. Mater. Sci. 31, 225–236.

Guo, Z.K., Kobayashi, A.S., Hay, J.C., White, K.W., 1999. Fracture process zone modeling of monolithic Al_2O_3. Eng. Fract. Mech. 63 (2), 115–129.

Harris, P.J.F., 2004. Carbon nanotube composites. Int. Mater. Rev. 49 (1), 31–43.

Hong, S.S., Kim, K.S., 2003. Extraction of cohesive-zone laws from elastic far-fields of a cohesive crack tip: a field projection method. J. Mech. Phys. Solids 51 (7), 1267–1286.

Huang, Y., Gao, H., 2001. Intersonic crack propagation. Part I: The fundamental solution. J. Appl. Mech. 68, 169–175.

Kubair, D.V., Geubelle, P.H., Huang, Y., 2002. Intersonic crack propagation in homogeneous media under shear-dominated loading: theoretical analysis. J. Mech. Phys. Solids 50, 1547–1564.

Kubair, D.V., Geubelle, P.H., Huang, Y., 2003. Analysis of a rate-dependent cohesive model for dynamic crack propogation. Eng. Fract. Mech. 70, 685–704.

Lau, K.T., Shi, S.Q., 2002. Failure mechanisms of carbon nanotube/epoxy composites pre-treated in different temperature environments. Carbon 40, 2965–2968.

Li, V.C., Chan, C.M., Leung, K.Y., 1987. Experimental determination of the tension-softening relations for cementitious composites. Cement Concrete Res. 17, 441–452.

Li, C.Y., Chou, T.W., 2003. Multiscale modeling of carbon nanotube reinforced polymer composites. J. Nanosci. Nanotechnol. 3 (5), 423–430.

Liao, K., Li, S., 2001. Interfacial characteristics of a carbon nanotube–polystyrene composite system. Appl. Phys. Lett. 79 (25), 4225–4227.

Liu, Y.J., Chen, X.L., 2003. Evaluations of the effective material properties of carbon nanotube-based composites using a nanoscale representative volume element. Mech. Mater. 35, 69–81.

Lordi, V., Yao, N., 2000. Molecular mechanics of binding in carbon-nanotube-polymer composites. J. Mater. Res. 15, 2770–2779.

Maruyama, B., Alam, H., 2002. Carbon nanotubes and nanofibers in composite materials. SAMPE J 38 (3), 59–70.

Mohammed, I., Liechti, K.M., 2000. Cohesive zone modeling of crack nucleation at bimaterials corners. J. Mech. Phys. Solids 48 (4), 735–764.

Namilae, S., Chandra, N., 2005. Multiscale model to study the effect of interfaces in carbon nanotube-based composites. J. Eng. Mater. Technol. 127, 222–232.

Needleman, A., 1987. A continuum model for void nucleation by inclusion debonding. J. Appl. Mech. 54, 525–531.

Odegard, G.M., Gates, T.S., Nicholson, L.M., Wise, K.E., 2002. Equivalent-continuum modeling of nano-structured materials. Compos. Sci. Technol. 62, 1869–1880.

Odegard, G.M., Gates, T.S., Wise, K.E., Park, C., Siochi, E.J., 2003. Constitutive modeling of nanotube-reinforced polymer composites. Compos. Sci. Technol. 63, 1671–1687.

Rapaport, D.C., 2004. The Art of Molecular Dynamics Simulation. Cambridge University Press, Cambridge.

Samudrala, O., Huang, Y., Rosakis, A.J., 2002. Subsonic and intersonic mode II crack propagation with a rate-dependent cohesive zone. J. Mech. Phys. Solids 50, 1231–1268.

Samudrala, O., Rosakis, A.J., 2003. Effect of loading and geometry on the subsonic/intersonic transition of a bimaterial interface crack. Eng. Fract. Mech. 70, 309–337.

Schadler, L.S., Giannaris, S.C., Ajayan, P.M., 1998. Load transfer in carbon nanotube epoxy composites, Appl. Phys. Lett. 73 (26), 3842–3844.

Shi, D.L., Feng, X.Q., Huang, Y., Hwang, K.C., Gao, H., 2004. The effect of nanotube waviness and agglomeration on the elastic property of carbon nanotube-reinforced composites. J. Eng. Mater. Technol. 126, 250–257.

Tan, H., Huang, Y., Liu, C., Geubelle, P.H., 2005a. The Mori–Tanaka method for composite materials with nonlinear interface debonding. Int. J. Plasticity 21 (10), 1890–1918.

Tan, H., Liu, C., Huang, Y., Geubelle, P.H., 2005b. The cohesive law for the particle/matrix interfaces in high explosives. J. Mech. Phys. Solids 53 (8), 1892–1917.

Tan, H., Liu, C., Huang, Y., Geubelle, P.H., 2006. The effect of nonlinear interface debonding on the constitutive model of composite materials. Int. J. Multiscale Comput. Eng. (in press).

Thiagarajan, G., Hsia, K.J., Huang, Y., 2004a. Finite element implementation of virtual internal bond model for simulating crack behavior. Eng. Fract. Mech. 71, 401–423.

Thiagarajan, G., Huang, Y., Hsia, K.J., 2004b. Fracture simulation using an elasto–viscoplastic virtual internal bond model with finite element. J. Appl. Mech. 71, 796–804.

Thostenson, E.T., Ren, Z.F., Chou, T.W., 2001. Advances in the science and technology of carbon nanotubes and their composites: a review. Compos. Sci. Technol. 61, 1899–1912.

Thostenson, E.T., Chou, T.W., 2003. On the elastic properties of carbon nanotube-based composites: modelling and characterization. J. Phys. D-Appl. Phys. 36 (5), 573–582.

Thostenson, E.T., Li, C.Y., Chou, T.W., 2005. Nanocomposites in context. Compos. Sci. Technol. 65 (3–4), 491–516.

Wong, M., Paramsothy, M., Xu, X.J., Ren, Y., Li, S., Liao, K., 2003. Physical interactions at carbon nanotube-polymer interface. Polymer 44, 7757–7764.

Zhang, P., Klein, P.A., Huang, Y., Gao, H., Wu, P.D., 2002. Numerical simulation of cohesive fracture by the Virtual-Internal-Bond model. Comput. Model. Eng. Sci. 3, 263–277.